

RESEARCH

Open Access



Chromatin interaction analysis reveals changes in small chromosome and telomere clustering between epithelial and breast cancer cells

A. Rasim Barutcu¹, Bryan R. Lajoie², Rachel P. McCord², Coralee E. Tye⁵, Deli Hong^{1,5}, Terri L. Messier⁵, Gillian Browne⁵, Andre J. van Wijnen⁴, Jane B. Lian⁵, Janet L. Stein⁵, Job Dekker^{2,3}, Anthony N. Imbalzano¹ and Gary S. Stein^{5*}

Abstract

Background: Higher-order chromatin structure is often perturbed in cancer and other pathological states. Although several genetic and epigenetic differences have been charted between normal and breast cancer tissues, changes in higher-order chromatin organization during tumorigenesis have not been fully explored. To probe the differences in higher-order chromatin structure between mammary epithelial and breast cancer cells, we performed Hi-C analysis on MCF-10A mammary epithelial and MCF-7 breast cancer cell lines.

Results: Our studies reveal that the small, gene-rich chromosomes chr16 through chr22 in the MCF-7 breast cancer genome display decreased interaction frequency with each other compared to the inter-chromosomal interaction frequency in the MCF-10A epithelial cells. Interestingly, this finding is associated with a higher occurrence of open compartments on chr16–22 in MCF-7 cells. Pathway analysis of the MCF-7 up-regulated genes located in altered compartment regions on chr16–22 reveals pathways related to repression of WNT signaling. There are also differences in intra-chromosomal interactions between the cell lines; telomeric and sub-telomeric regions in the MCF-10A cells display more frequent interactions than are observed in the MCF-7 cells.

Conclusions: We show evidence of an intricate relationship between chromosomal organization and gene expression between epithelial and breast cancer cells. Importantly, this work provides a genome-wide view of higher-order chromatin dynamics and a resource for studying higher-order chromatin interactions in two cell lines commonly used to study the progression of breast cancer.

Keywords: Hi-C, Chromosome Conformation Capture, Breast Cancer, Topologically Associating Domain, TAD, Telomere

Background

Three-dimensional genome organization is important for regulation of gene expression by bringing together distant promoter, enhancer and other *cis*-regulatory regions [1–3]. The development of cancer involves several genetic and epigenetic alterations that result in aberrant gene expression [4–7]. Moreover, cancer is a disease characterized by major morphological changes in the nucleus that are used as diagnostic markers [8, 9]. Even though the morphological features of cancer are well

characterized, the molecular consequences of the aberrant nuclear morphology are still poorly understood.

The higher-order folding of chromatin within the nucleus involves hierarchical structures spanning different length scales [10]. Microscopic imaging shows that chromosomes are positioned within confined volumes known as chromosome territories [11]. In the nucleus, each chromosome has a preferred, but not fixed, position in which gene-dense chromosomes tend to be at the nuclear interior whereas the gene-poor chromosomes are found near the nuclear periphery [11–14]. Increasing evidence highlights the importance of chromosome and gene positioning during breast cancer initiation [15–17]. Moreover, recent evidence demonstrates the influence of

* Correspondence: gary.stein@uvm.edu

⁵Department of Biochemistry and University of Vermont Cancer Center, University of Vermont College of Medicine, 89 Beaumont Avenue, Burlington, VT 05405, USA

Full list of author information is available at the end of the article

physical spatial proximity in the nucleus on recurrent translocations [18–20].

Several studies have revealed that chromosome territories consist of megabase-scale genomic compartments that are either euchromatic, gene-rich, and highly transcribed (A-type compartments) or heterochromatic, gene-poor, and silent (B-type compartments) [20–23]. The open and closed compartments mostly interact with other open and closed compartments, respectively, whereas there are very few interactions between the two different types of compartments. The open (A-type) compartments preferentially and spatially cluster together in the nuclear interior, whereas the closed (B-type) compartments cluster together near the nuclear periphery [14].

Compartments are composed of 100 kb to 1 Mb scale topologically associating domains (TADs). TADs have been defined as clusters of interactions, in which the enhancers and promoters of co-regulated genes cross-talk with one another. Intra-TAD interactions are much more prevalent than inter-TAD interactions [24]. TADs have been shown to be largely invariant across different species, cell types, and physiological conditions [24, 25] and may act as functional units for transcription regulation [26–28]. Recent work elucidated the role of TADs and transcription factor-associated interactions at a genome-wide level in the context of hormonal regulation (i.e., estrogen or progesterone treatment) [28–35]. TADs are thought to facilitate transcriptional regulation by integrating the regulatory activities within the same domain [10, 26]. Within TADs, looping interactions at the 10 kb to 1 Mb scale bring together enhancers and promoters to regulate gene expression. Functional characterization of long-range interactions in breast cancer has been studied within certain candidate regions [36–40] or by examining the genome-wide interactions of a single locus using more unbiased approaches [41–43]. Probing chromatin structure in cancer has potential as a discovery tool for identifying candidate biomarkers [44], as the organization of the chromatin is often perturbed at different hierarchical levels in cancer [45]. Despite the number of previous studies, differences in genome-wide chromatin structure between normal epithelial cells and tumorigenic breast cancer cells remain unknown.

In this study, in order to characterize different scales of genome organization during breast cancer development, we performed genome-wide chromosome conformation capture (Hi-C) analyses in MCF-10A mammary epithelial and MCF-7 tumorigenic breast cancer cells. Hi-C is a powerful molecular tool to probe genome-wide chromatin interactions in an unbiased way [46]. Our results uncovered fundamental differences of chromatin organization at different genomic scales between two commonly used mammary epithelial and tumorigenic breast cancer cell lines. This work provides

an important foundation for understanding the relationship between the alterations in chromatin organization and gene expression in breast cancer.

Results

Small, gene-rich chromosomes interact less frequently in the MCF-7 breast cancer genome

In order to probe the genome-wide chromatin structure of mammary epithelial and breast cancer cells, we generated Hi-C libraries from two independent biological replicates for the MCF-10A and MCF-7 cell lines. After sequence filtering [47], a total of ~152 and ~143 million interactions were obtained from the MCF-10A and MCF-7 combined replicate Hi-C libraries, respectively (Figure S1 in Additional file 1), with high reproducibility between the biological replicates (Figure S2 in Additional file 1). For the initial Hi-C analyses, we used the iterative correction method (ICE) [48] to correct for systematic biases, including copy number differences.

Genome-wide interaction data were visualized as chromosome versus chromosome heat maps, where darker colors represent more frequent interaction events (Fig. 1a, b). The heat maps revealed two aspects of large-scale genome organization in the MCF-10A and MCF-7 cells. First, consistent with the notion of chromosome territories [11], intra-chromosomal interactions (visualized as darker boxes along the diagonal) were much more frequent than inter-chromosomal interactions (Fig. 1a, b). Second, we observed a number of large blocks of inter-chromosomal interactions representing the translocation events in these cell lines. Comparing the translocated regions in the Hi-C data with previously published MCF-10A and MCF-7 spectral karyotyping (SKY) and multiplex fluorescence in situ hybridization (M-FISH) data [49, 50], we observed that the majority of the translocated regions identified by SKY/M-FISH were also identified by Hi-C (Figures S3 and S4 in Additional file 1).

In order to assess whether the clustering of chromosomes is altered between MCF-10A and MCF-7 cells, we compared the genome-wide interaction differences (see "Materials and methods"; Fig. 1c). Strikingly, we observed a strong physical proximity of gene-rich, small chromosomes (chr16–22) in MCF-10A compared with MCF-7 (Fig. 1a–c, lower panels). This interaction network of small chromosomes also included the p-arm of chr8 (Fig. 1c). Quantification of the inter-chromosomal interactions between chr16 through chr22, and between chr16 through chr22 and the rest of the genome revealed that there is a significant increase of inter-chromosomal associations between chr16 through chr22 in the MCF-10A genome (Fig. 1d). The same result was also observed when, as an alternative approach, a direct subtraction of the MCF-10A and MCF-7 interaction

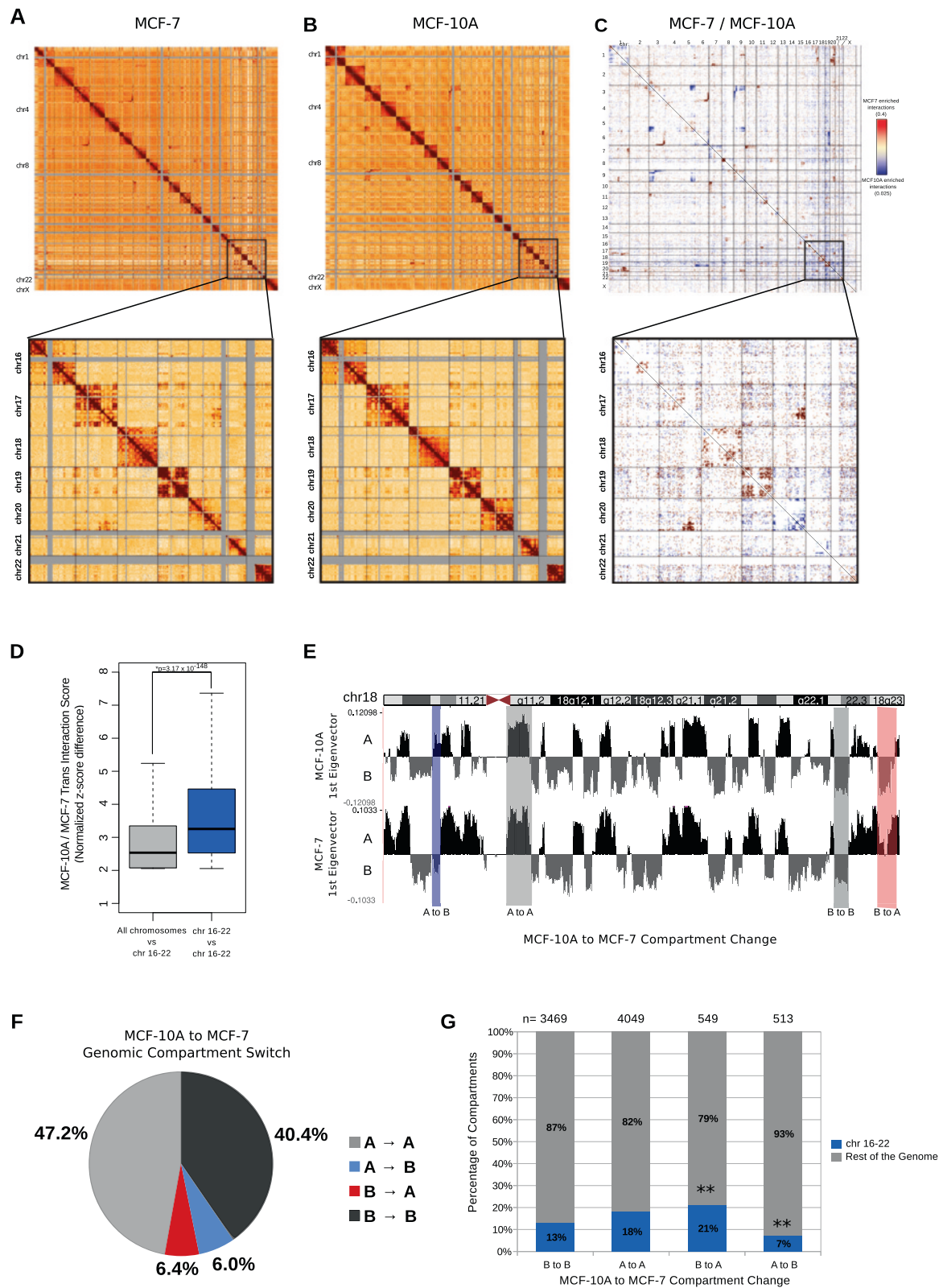


Fig. 1 (See legend on next page.)

(See figure on previous page.)

Fig. 1 Hi-C analyses identify that small chromosomes (chr16–22) in the MCF10A genome show preferential associations with each other. Genome-wide all-by-all 1-Mb Hi-C interaction heatmap of MCF-10A (**a**) and MCF-7 (**b**) cells. The chromosomes in all-by-all heatmaps are stacked from *top left to bottom right* in order (chr1, chr2...chr22 and chrX). The *gray regions* indicate repetitive regions (such as centromeres) in which the sequencing reads could not be mapped. *Intra-chromosomal* interactions were much more frequent than inter-chromosomal interactions. The blocks of enriched inter-chromosomal interactions represent the translocated regions. In the *lower panels*, enlargements of the *cis-* and *trans-*interactions for chr16 through chr22 are shown. **c** Genome-wide heatmap of significant differential interactions between MCF-10A and MCF-7. Each *dot* denotes a genomic region of 6.5 Mb. Chromosomes are stacked from *top left to bottom right* from chr1 through chr22 and chrX. The *red color* indicates MCF-7-enriched interactions and the *blue color* indicates MCF-10A-enriched interactions. The *white regions* denote interacting regions that are not significantly changed between the cell lines. In the *lower panel*, significant interactions within and between chr16–22 are shown. **d** Boxplot showing the MCF-10A/MCF-7 inter-chromosomal interaction frequency differences between chr16 through chr22 and all the other chromosomes (*grey*) or between chr16 through chr22 (*blue*). The *p* value was determined using Wilcoxon rank-sum test. **e** First principal component of chr18, representing the open A-type (*black*) and closed B-type (*grey*) compartmentalization. *Highlighted bars* represent examples of regions with either stable or differential compartmentalization. The differential compartments are defined as genomic regions in which one type of compartmentalization is observed in one cell line and the other compartment type in the second cell line. **f** Pie chart showing the genomic compartment changes between MCF-10A and MCF-7 genomes. "A" and "B" denote the open and closed compartments, respectively. "A → A" represents compartments that are open in both cell lines, "B → B" represents compartments that are closed in both cell lines, "A → B" denotes compartments that are open in MCF-10A but closed in MCF-7, and "B → A" denotes compartments that are closed in MCF-10A and open in MCF-7. **g** Bar graph showing the percentage of compartments that have switched (A → B or B → A) or remained similar (A → A or B → B) between MCF-10A and MCF-7 genomes for chr16 through chr22 (*blue*) and the rest of the genome (*grey*). Chr16–22 display a higher percentage of B → A compartment switching, and a lower percentage of A → B compartment switching between MCF-10A and MCF-7, suggesting a more open compartmentalization in MCF-7. ****P** value < 0.001: Chi-square with Yates' correction

matrices was performed (Figure S5a, b in Additional file 1). Moreover, the larger chromosomes (chr1–15 and X) in the MCF-10A genome showed similar levels of differential interaction frequency with other large chromosomes or chr16–22. Consistent with this observation, the positioning of chr18 with other small chromosomes was not prevalent in the raw Hi-C interaction matrices (Figure S6a–c in Additional file 1). However, the relative (MCF-10A/MCF-7) interaction frequency of chr18 with other small chromosomes was significantly increased in the MCF-10A cells (Figure S6d, e in Additional file 1), which suggests that all of the small chromosomes in MCF-10A cells show increased proximity to each other compared with the relative proximity in the MCF-7 cancer cell line.

Decreased interaction frequency between small chromosomes in MCF-7 cells coincides with increased open chromatin compartmentalization

Previous evidence [21] has shown there are two unique patterns of interactions in the genome, representing the open (A-type) and closed (B-type) genomic compartments. We identified the two patterns of compartmentalization in both genomes with high reproducibility among the biological replicates (see "Materials and methods"; Figure S7a, b in Additional file 1). Associating the MCF-7 ENCODE ChIP-seq datasets with the genomic compartments revealed the known features of genomic compartmentalization, including increased DNase I hypersensitivity, and higher levels of transcription factor binding in open (A-type) compartments in the MCF-7 genome (Figure S7c, d in Additional file 1).

To determine whether there are any differences in the compartmentalization between the MCF-10A and MCF-7 genomes, we compared the compartments throughout the genome at 250 kb resolution. The MCF-10A and MCF-7 genomes displayed similar distribution of open and closed compartments, with certain regions showing a change in genomic compartmentalization from A-type to B-type and vice versa (Fig. 1e, f). The majority of compartments were the same in both cell lines, where 47 % of all compartments constituted the A-type compartments and 40 % constituted the B-type compartments (Fig. 1f). Compartment switching was homogeneous throughout the chromosomes, rather than in a few hot spots (Figure S7e in Additional file 1).

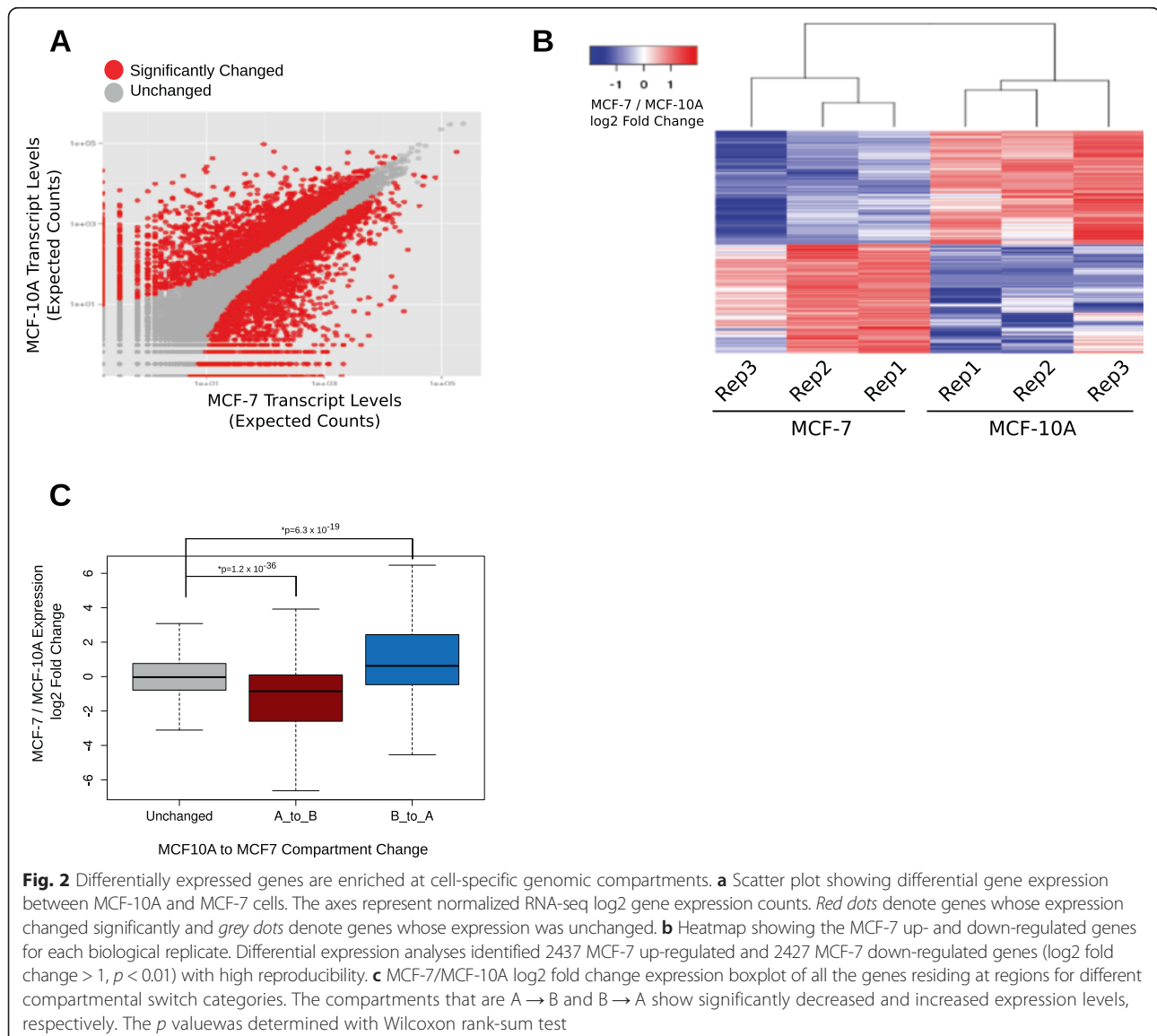
Importantly, 12 % of all compartments in the MCF-10A genome transitioned to the opposite compartment (A-type to B-type and vice versa) in MCF-7 cells (Fig. 1f). To understand if the inter-chromosomal interaction changes we observed between small chromosomes were related to any compartment change, we asked whether there was an enrichment in transition of genomic compartments on small chromosomes (chr16–22). We found a significant enrichment of genomic regions on chr16–22 that switched to the A-type compartment in MCF-7 cells from the B-type compartment in MCF-10A cells (Fig. 1g). Conversely, we also observed a significant decrease of compartment transition from A-type in MCF-10A to B-type in MCF-7 on small chromosomes (Fig. 1g). These findings show that there is a higher frequency of open compartments on small chromosomes in the MCF-7 genome, which suggests a relationship between inter-chromosomal clustering, compartmentalization and phenotypic gene expression.

Decreased inter-chromosomal interactions and higher frequency of open compartmentalization on chr16–22 in MCF-7 cells are associated with WNT signaling-related genes

Open compartmentalization is correlated with increased gene expression. We asked if the differential interaction network and compartmentalization of chr16 through chr22 between MCF-10A and MCF-7 cells are associated with differential gene expression. First, to characterize the gene expression differences between MCF-10A and MCF-7 cells, we performed RNA-seq with ribosomal RNA-depleted RNA from MCF-10A and MCF-7 cells with biological triplicates (Figure S8a, b in Additional file 1). Differential expression analyses identified 2437 MCF-7 up-regulated and 2427 MCF-7 down-regulated genes (\log_2 fold change > 1 , $p < 0.01$) with high reproducibility

(Fig. 2a, b). The number of differentially expressed genes identified in this study is comparable to previously published microarray studies [51]. The significant expression changes were enriched for the medium to highly expressed genes (Figure S8c in Additional file 1). The gene ontology terms associated with MCF-7 down-regulated (i.e., MCF-10A over-expressed) genes included terms such as “hemidesmosome assembly”, “focal adhesion”, and “neutral lipid biosynthetic process” (Additional file 2). On the other hand, gene ontology terms associated with MCF-7 up-regulated genes included terms such as “calcium-dependent cell adhesion” (Additional file 2).

To test the link between genome-wide open spatial compartmentalization and increased gene expression more directly, we analyzed the frequency of differentially



expressed genes at regions where a compartment transition is observed. In agreement with previous findings [52], MCF-7 down-regulated genes were enriched in regions where the open A-type compartment in MCF-10A transitioned to a closed B-type compartment in MCF-7 (Fig. 2c). Conversely, there was an enrichment of MCF-7 up-regulated genes in regions with a B-type compartment in MCF-10A that switched to an A-type compartment in MCF-7 (Fig. 2c). In other words, when the MCF-7/MCF-10A log₂ fold change expression levels were plotted for each compartment change category, we observed a down-regulation of MCF-7 genes in A-type to B-type compartment switch regions and an up-regulation of MCF-7 genes in B-type to A-type switch regions, respectively (Fig. 2c). These results show that compartment changes in the genome reflect differential gene expression.

Finally, to assess whether the differences in interactions and genomic compartments among the small chromosomes are associated with altered gene expression, we focused on the MCF-7 up-regulated genes on small chromosomes where the compartmentalization was switched from B-type to A-type (MCF-10A to MCF-7). REACTOME pathway analysis of these genes revealed well known oncogenic pathways, including “repression of WNT target genes” and “TCF/LEF binding to gene promoters” (Additional file 3).

Taken together, these results suggest that the decrease of inter-chromosomal associations of small chromosomes in the MCF-7 genome is associated with a higher open compartmentalization in MCF-7 and expression of genes related to the WNT signaling pathway, which is frequently implicated in tumorigenesis.

Cell-line specific TAD boundaries are conserved between MCF-10A and MCF-7

Chromosome conformation capture-based studies revealed that A-type and B-type compartments are composed of TADs, where the expression levels of the genes in a single TAD can be co-regulated [24, 28, 53]. TADs have been shown to be stable units in different species, cell types, and physiological conditions [24, 28]. However, whether the large-scale chromosomal interactions and altered genomic compartments observed between MCF-10A and MCF-7 genomes have an effect on the structure of the underlying TAD formation and ultimately on gene expression is unknown. To address this question, we identified the TAD boundaries by calculating the insulation plot of the 40 kb resolution genome-wide interaction maps (see “Materials and methods”; Figure S9a in Additional file 1), with high reproducibility between the biological replicates (Figure S9b in Additional file 1). We detected 3305 and 3272 TAD boundaries in MCF-10A and MCF-7 genomes, respectively.

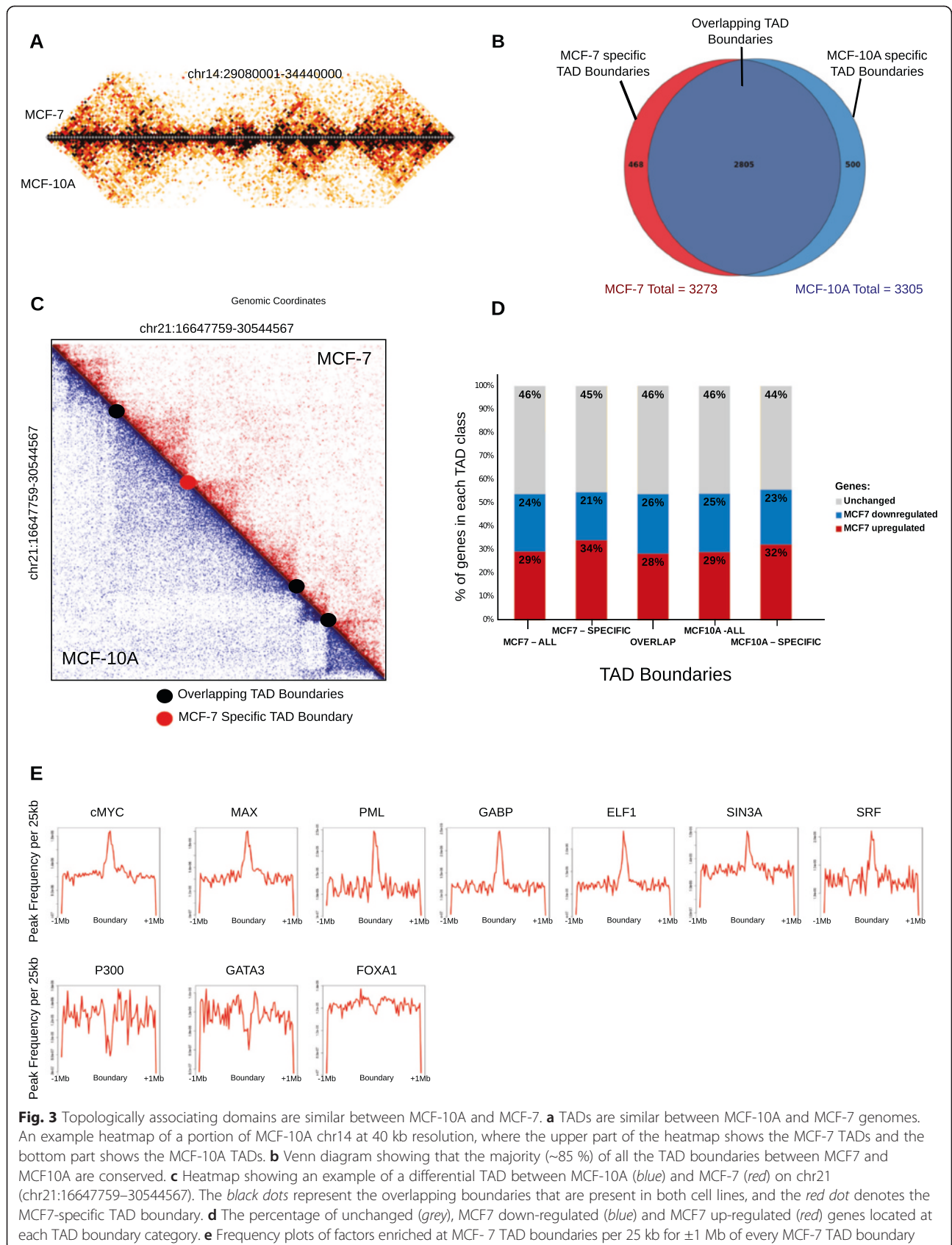
Despite the differences in chromosomal structure and changes in compartmentalization and gene expression, ~85 % (2805) of the TAD boundaries were common between the cell lines (Fig. 3a, b). This rate of TAD boundary overlap is consistent with previous comparisons in different cell types and conditions [24, 28]. This result suggests that despite having cell type-specific translocations and large-scale structural differences, TAD boundaries are consistent between non-tumorigenic and tumorigenic cells.

Closer examination of TAD boundaries revealed that several TADs were “broken” into multiple sub-TADs between the cell lines. The boundaries that were shared among the larger and smaller TADs between the cell lines were categorized as “overlapping”, and the boundaries that were unique to a cell line were categorized as “cell line-specific” boundaries (Fig. 3c). We asked whether the genes residing at the cell line-specific boundaries showed cell line-specific differential gene expression. When the percentages of unchanged and MCF-7 up- and down-regulated genes were plotted per TAD boundary category, we did not find a strong correlation between cell type-specific TAD boundaries and differential gene expression (Fig. 3d).

As well as the TAD boundaries, we also analyzed the TADs. We categorized the TADs as overlapping (>90 % overlap), MCF-7-specific or MCF-10A-specific (see “Materials and methods” and below) (Figure S10a in Additional file 1). The overlapping TADs were slightly larger in size than the cell line-specific TADs (Figure S10b in Additional file 1). We then asked whether cell line-specific TADs showed differential gene expression. Analysis of differential gene expression for each TAD category showed that cell type-specificity of the TADs was not correlated with cell type-specific gene expression (Figure S10c in Additional file 1).

MCF-7 TAD boundaries are enriched for several oncoproteins

TAD boundaries are bound by multiple factors [24, 54]. To investigate the chromatin states of the boundaries, we calculated the enrichment of factors characterized by MCF-7 ENCODE datasets at the MCF-7 TAD boundaries (Fig. 3e; Figure S10d in Additional file 1). The known features of the TAD boundaries, such as the enrichment of H3K36me₃, CTCF, RAD21, transcription start sites, POL2, and DNase I hypersensitive sites, and the depletion of H3K9me₃, were observed at the MCF-7 TAD boundaries (Figure S10d in Additional file 1). Interestingly, we observed a strong association of GABP, ELF1, PML, SIN3A, SRF, and the oncogenic drivers cMYC and MAX at MCF-7 TAD boundaries, and a depletion of GATA3 and FOXA1 (Fig. 3e). Consistent with previous work [24], P300 was depleted at the MCF-7 boundary



regions. The rest of the MCF-7 ENCODE datasets did not show any enrichment (data not shown).

Recent evidence suggested that TADs may act as stable units of replication domains [55]. Therefore, we intersected the previously published MCF-7 Repli-seq dataset [55] with MCF-7 TAD boundaries and, consistent with the literature, we determined that late replicating regions were depleted at TAD boundary regions (Figure S11a in Additional file 1). Moreover, expression quantitative trait loci (eQTLs) have been shown to be preferentially located at TAD boundaries [56]. Integrating the breast cancer eQTL data [57] with MCF-7 TAD boundaries, we determined that breast cancer-associated eQTLs were enriched in overlapping TAD boundaries (Figure S11b in Additional file 1). Altogether, these results uncover previously unidentified transcription factors and chromatin states that may potentially play roles at the TAD boundaries.

The telomeric/sub-telomeric regions in the MCF-10A genome display stronger associations than those in the MCF-7 genome

Previous evidence has shown that interaction frequency decreases as a function of genomic distance [21]. This phenomenon represents the nature of the chromatin fiber and is a reflection of the folding status of the underlying chromatin [58]. We first asked whether the fiber characteristics of the MCF-10A and MCF-7 genomes were similar. Scaling plots of 1 Mb binned genome-wide intra-chromosomal interactions displayed the expected exponential decrease of contact probability as a function of increasing genomic distance in both MCF-10A and MCF-7 cells (Fig. 4a). Surprisingly, and in contrast to all previously published human Hi-C datasets, the frequency of interactions in MCF-10A showed an increase at very large genomic distances (>200 Mb; Fig. 4a). This suggests that very distant (i.e., telomeric/sub-telomeric) regions of chromosomes show a higher interaction frequency on the same chromosome. To assess whether the telomeric ends of the chromosomes in MCF-10A indeed have higher frequencies of interactions compared with those in MCF-7, we calculated the intra-chromosomal interaction frequency of the ends of each chromosome (5 % by length) in MCF-10A and MCF-7 cells. We observed a significant increase in telomeric/sub-telomeric interaction frequency in the MCF-10A genome (Fig. 4b), which supports the observation that intra-chromosomal telomeric interactions are more frequent in MCF-10A cells. Scaling plots of each chromosome individually at 250 kb resolution indicate that the increase in telomeric/sub-telomeric interactions seemed to be driven by chr1, chr2, and chr7 in the MCF-10A genome (Fig. 4c–e; Figure S12 in Additional file 1). However, this phenomenon was not observed on other

large chromosomes in MCF-10A cells, such as chr3 (Fig. 4f; Figure S12 in Additional file 1). Certain chromosomes, such as chr11 and chr16, showed increased interaction frequency at large distances in both the MCF-10A and MCF-7 genomes even though their lengths did not span 200 Mb (Figure S12 in Additional file 1). As expected, this was not observed when the scaling plots for individual chromosomal arms were analyzed (Fig. 4g–i; Figure S13 in Additional file 1).

These results suggest that the telomeric ends of the chromosomes, especially chr1, chr2, and chr7, in the MCF-10A genome are in closer proximity than those in MCF-7. Taken together, we identified large-scale differences in both *cis*- and *trans*-chromosomal interactions between two commonly used cell lines in breast cancer research.

Discussion

Cancer is a disease characterized by major morphological changes in the nucleus [8, 9]. Although individual gene positioning may differ [16], the relative arrangement of chromosomes in the interphase nucleus can be conserved between normal and cancer cells [59]. Furthermore, extensive epigenetic dysregulation is observed in the cancer state. In order to map the genome-wide interactions and perform a comparative analysis, we performed Hi-C in the MCF-10A and MCF-7 cell lines. We observed a higher background interaction frequency in the MCF-7 genome compared with the MCF-10A genome (Fig. 1a, b). This background could be the result of a technical source (i.e., the ligation step in the Hi-C procedure) or because of increased background interaction frequency in the MCF-7 genome due to the probabilistic positioning of the chromosomes inside the aneuploid nucleus and increased diversity of interactions within this genome.

Comparison of MCF-7 and MCF-10A Hi-C data revealed a significant depletion of inter-chromosomal associations between small, gene-rich chromosomes (chr16–22) in the MCF-7 genome. One possibility for the loss of interactions among the small chromosomes in MCF-7 compared with MCF-10A cells is that randomization (i.e., loss of specificity) of contacts within the MCF-7 genome could lead to lower frequencies of individual contacts, and hence to an apparent loss of interaction. However, loss of specific contacts does not itself cause a difference in overall chromosome contacts. Two whole chromosomes that tend to be close together in a cell will overall show more inter-chromosomal interactions with each other by Hi-C than will two distant chromosomes, even if they have no specific interactions that are consistent across the population of cells. If each cell in the population has a different arrangement of chromosome territories, this will look, on average, like

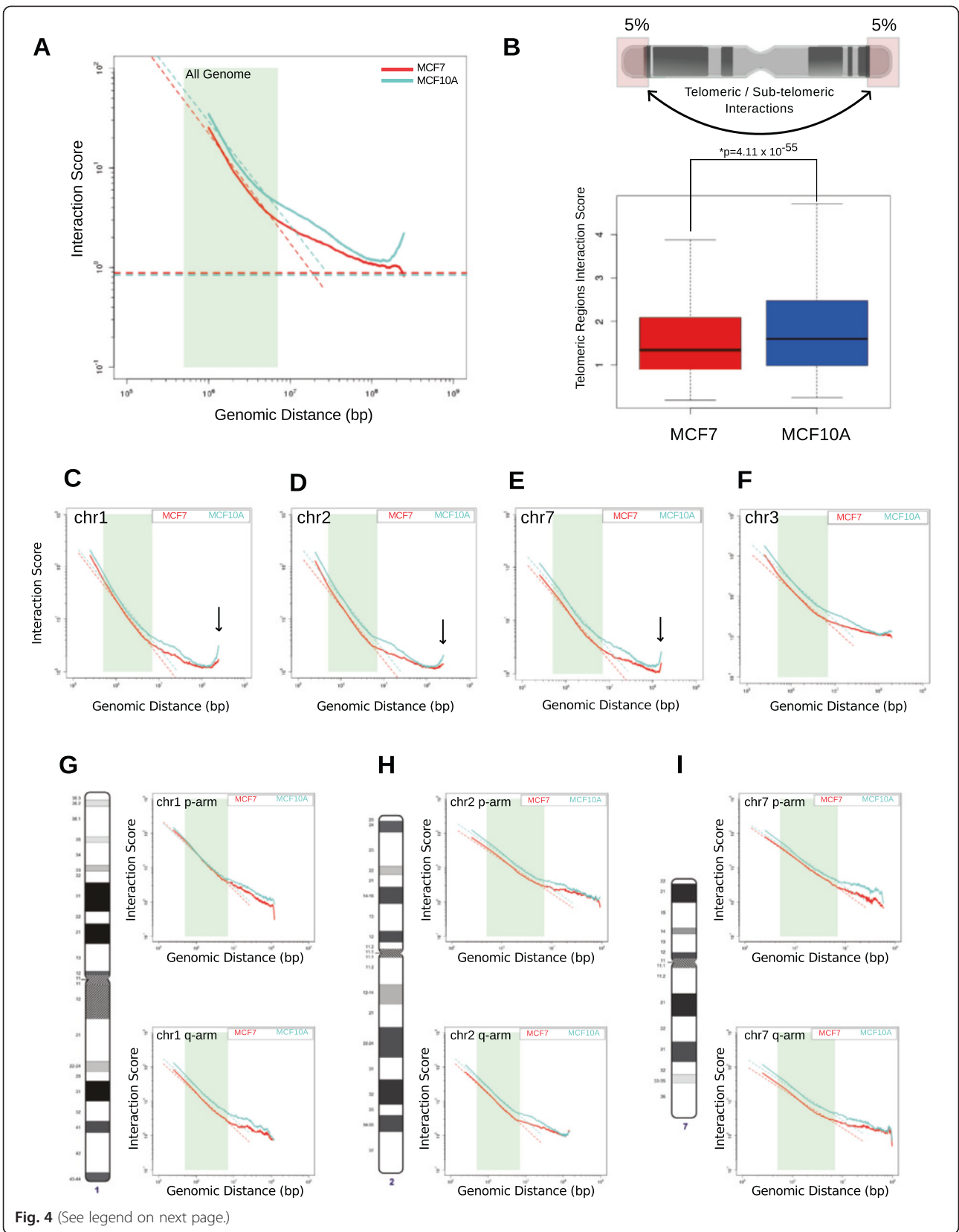


Fig. 4 (See legend on next page.)

(See figure on previous page.)

Fig. 4 Telomeric and sub-telomeric regions in the MCF-10A genome display increased interaction frequencies. **a** Scaling plot of interaction frequencies against genomic distance for the MCF7 and MCF10A genomes. The MCF10A genome showed increased interaction frequency at genomic distances >200 Mb, suggesting telomere/sub-telomere associations. **b** Quantification of the interaction frequency between the telomeric regions (5 % of the ends by length) of each chromosome in MCF7 and MCF10A. The *p* value was determined by Wilcoxon rank-sum test. Scaling plots of MCF-10A and MCF-7 for chr1 (**c**), chr2 (**d**), chr7 (**e**), and chr3 (**f**). Chromosomes 1, 2 and 7 displayed an increased interaction frequency at large distances in MCF-10A but chromosome 3 did not. Scaling plots of individual chromosome arms for chr1 (**g**), chr2 (**h**), and chr7 (**i**)

less clustering of small chromosomes. But this scenario should also reveal more interactions between large and small chromosomes and less clustering of large chromosomes. In Figure S5 in Additional file 1 and Fig. 1c, in contrast, we do not observe a compensating increase in interactions between the small and large chromosomes, suggesting that this is not just a randomization of interactions. Moreover, it should be kept in mind that there are several extensive rearrangements in the MCF-7 genome, and it could be that only the re-arranged copies of a highly aneuploid chromosome may show a particular three-dimensional conformation.

The decreased clustering of small chromosomes and the differentially open compartmentalized regions in MCF-7 are associated with increased expression of genes related to tumorigenesis. The correlation between increased gene expression in B-type to A-type compartment switch regions and a higher number of A-type compartments on chr16–22 in MCF-7 cells suggests that the underlying mechanism for this phenomenon is most likely due to transcriptional differences, rather than chromosomal copy number changes between the cell lines. The loss of small chromosome clustering may also be interpreted as a reflection of mis-organization of the chromosome territories in cancer.

Genomic compartmentalization has been shown to be associated with gene expression [21, 52]. One hypothesis for the clustering, compartmental, and transcriptional changes we observe in small chromosomes would be that once a gene is activated/repressed in the process of tumorigenesis, its position in the three-dimensional nuclear space is changed, with movement towards the open/closed compartment regions. Such a phenomenon has been previously shown by microscopic studies [60]. An alternative hypothesis is that chromosomes change compartments before gene expression changes. A recent study supports the alternative hypothesis in which chromatin decondensation plays a major role in cell differentiation [61].

Scaling plot analysis (Fig. 4) suggested that distinct types of chromatin folding states might exist between MCF-10A and MCF-7 cells, both genome-wide and at individual chromosomes [58]. Surprisingly, and in contrast to all previous human Hi-C datasets, there was an increased frequency of interactions at distances >200 Mb in MCF-10A cells, suggesting interactions between

telomeric and sub-telomeric regions on the same chromosome. It has been suggested that telomere clustering is associated with the alternate lengthening of telomeres (ALT) mechanism [62]. ALT is a mechanism in which telomere length is maintained through a homologous recombination-dependent process. It could be possible that the MCF-10A and MCF-7 cells have different mechanisms of telomere maintenance, and the proximity of telomeric ends in the MCF-10A genome might suggest an effect of increased ALT regulation. Increased telomere interactions were observed in chr1, chr2, and chr7, and on some smaller chromosomes (Figure S12 in Additional file 1), but not in individual chromosomal arms (Figure S13 in Additional file 1). A recent report suggests that 10 % of all cancers and immortalized cell lines display the ALT mechanism [63]. Our results are consistent with previous findings that the presence of an ALT mechanism results in clustering of telomeres, which is observed in epithelial MCF-10A cells but not in tumorigenic MCF-7 cells.

Overall, in this study we charted the chromatin structure of mammary epithelial and breast cancer cells at different chromosomal scales, from large-scale chromosomal *cis*- and *trans*-interactions to genomic compartmentalization and TAD formation (Figure S14 in Additional file 1). Further studies on normal and cancer genomes and primary cells will provide additional insight into the functional role of chromatin organization in transcriptional regulation and tumorigenesis.

Conclusions

This study provides a genome-wide molecular view of alterations in the three-dimensional chromatin organization between epithelial and breast cancer cells.

Materials and methods

Cell culture

MCF-10A cells were obtained from the Barbara Ann Karmanos Cancer Institute (Detroit, MI, USA). The cells were maintained in monolayer in Dulbecco's modified Eagle's medium-F12 (DMEM/F12; Invitrogen, 21041025) supplemented with 5 % horse serum (Invitrogen, 16050122), 1 % penicillin/streptomycin (Invitrogen, 15140122), 0.5 µg/ml hydrocortisone (Sigma, H-0888), 100 ng/ml cholera toxin (Sigma, C-8052), 10 µg/ml insulin (Sigma, I-1882), and 20 ng/ml recombinant

human epidermal growth factor (Peprotech, 100–15) as previously described [64]. MCF-7 cells were obtained from ATCC and were cultured in DMEM supplemented with 10 % fetal bovine serum and penicillin/streptomycin.

RNA-seq and analysis

The RNA-seq libraries were generated with TruSeq Stranded Total RNA with Ribo-Zero Gold Kit and the samples were sequenced as 100-bp single-end reads using a Hi-Seq 2000 instrument. For the RNA-Seq analysis, the adapter sequences were first removed from the RNA-seq reads. Ribosomal RNA reads, if any, were filtered out using Bowtie [65]. After quality filtering and adapter removal steps, the reads were aligned to a transcriptome and quantified using RSEM v.1.2.7 [66]. The annotation file was downloaded from University of California, Santa Cruz (UCSC) genome browser, human hg19 assembly. To quantify gene expression, gene counts and transcripts per million (TPM) were calculated by using the RSEM tool. Differential gene expression was calculated using the Deseq2 version 1.4.5 package in R 3.1.0 using the mean value of gene-wise dispersion estimates [67]. To find significant differentially expressed genes, we used 0.01 for adjusted p value and >1 log₂ fold change. Gene ontology analysis was performed with the FuncAssociate software [68]. The RNA-seq plots were confirmed using the ngs.plot software [69].

Preparation of Hi-C libraries

Hi-C was performed as previously described with minor modifications [46]. The modified part of the protocol was in the biotin incorporation step, where the mixture was incubated at 37 °C for 40 minutes with continuous shaking and tapping of the tube every 10 minutes. The MCF-10A and MCF-7 Hi-C samples displayed a range of 40–85 % biotin incorporation efficiency. At the end of Hi-C sample preparation, the libraries were sequenced using PE100 reads with a Hi-Seq 2000 instrument.

Read mapping/binning/ICE correction

Figure S1 in Additional file 1 summarizes the mapping results and different classes of reads and interactions observed [47]. The data were binned at 6.5-Mb, 1-Mb, 250-kb, 100-kb, and 40-kb non-overlapping genomic intervals. In our Hi-C analyses of the near diploid MCF-10A and aneuploidy MCF-7 cells, we utilized the iterative correction and eigenvector decomposition (ICE) method [48], which corrects for differences in copy number. A tetraploid chromosome may have twice as many sequenced interactions as a diploid chromosome, but the ICE method divides its final interaction counts by the total sum of all interactions and thus normalizes this difference. Iterative mapping and correction of Hi-C

data were performed as previously described [48]. Biological replicates showed high reproducibility (Pearson's correlation coefficient >0.9 for 1 Mb resolution data). Similarly, the first eigenvector comparison of the replicates showed high reproducibility (Figure S7a in Additional file 1). For the downstream analyses, sequences obtained from both biological replicates were pooled and ICE-corrected to serve as a combined dataset.

Z score calculation

We modeled the overall Hi-C decay with distance using a modified LOWESS method (alpha = 1 %, interquartile range filter), as described previously [70]. LOWESS calculates the weighted-average and weighted-standard deviation for every genomic distance and therefore normalizes for genomic distance signal bias.

Calculation of differential interactions

To capture the differences between MCF-10A and MCF-7 interactions, we first transformed the 6.5-Mb Hi-C data into Z score matrices for all four replicate datasets (MCF-7-R1, MCF-7-R2, MCF-10A-R1, and MCF-10A-R2). For each interaction, the mean sample:sample (between samples) Z score difference was calculated from all pairwise combinations of the four datasets (MCF-7-R1 and MCF-10A-R1, MCF-7-R1 and MCF-10A-R2, MCF-7-R2 and MCF-10A-R1, MCF-7-R2 and MCF-10A-R2). The replicate:replicate Z score difference (within samples) was also calculated for a random set of 500,000 interactions. These random replicate–replicate Z score differences were then used to build an expected distribution of Z score differences. The resulting Z score difference matrix was then derived by calculating for each bin the ratio of the mean of the set of four possible sample:sample Z score differences minus the genome-wide mean of the replicate:replicate Z score difference, divided by the genome-wide standard error of the replicate:replicate Z score differences. For Figure S5 in Additional file 1, we performed a direct subtraction of the Z score matrices (MCF-7 minus MCF-10A).

Compartment profiles

First, the Z scores of the interaction matrices at 250 kb resolution were generated as described previously [20]. Then, Pearson correlation on the Z score matrices was calculated. In performing principal component analysis [20, 21], the first principle component usually detects the patterns of increased and decreased interaction across the genome that appear as a “plaid pattern” in the heatmap. Each genomic region tends to match this prominent interaction pattern (positive eigenvector value) or its opposite (negative eigenvector value) and these represent the two spatially segregated compartments. In any given analysis, though, the generally open,

gene-rich A-type compartment may end up with either a positive or negative eigenvector. To detect which compartment is the open A-type and which is the closed B-type, the genome-wide gene density was calculated to assign the A-type and B-type compartmentalization.

Identification of TAD boundaries (insulation square analysis)

TAD calling was performed by calculating the “insulation” score of each bin using the 40 kb resolution combined Hi-C data. The mean of the interactions across each bin was calculated. By sliding a 1 Mb × 1 Mb (25 bins × 25 bins) square along the diagonal of the interaction matrix for every chromosome, we obtained the insulation score of the interaction matrix. Valleys in the insulation score indicate the depletion of Hi-C interactions occurring across a bin. These 40-kb valleys represent the TAD boundaries. Based on the variation of boundaries between replicates (Figure S9a in Additional file 1), we chose to add a total of 160 kb (80 kb to each side) to the boundary to account for replicate variation. The final boundaries span a 200-kb region. All boundaries with a boundary strength <0.15 were excluded as they were considered weak and non-reproducible. The insulation plots for the biological replicates showed high reproducibility (Pearson correlation coefficient = 0.80 for MCF-7 and 0.90 for MCF-10A replicates; Figure S9b in Additional file 1), suggesting the robustness of the method. Similarly, the overlap of detected boundaries also showed high reproducibility between the biological replicates (~85 % TAD boundary overlap for MCF-7 and ~91 % for MCF-10A). Therefore, we used the combined Hi-C replicates for the TAD analyses.

Identification of TADs

The cell line-specific TADs were identified using the bedtools suite [71]. First the boundaries on all chromosomes for both MCF-10A and MCF-7 were merged. The boundaries that overlapped were categorized as “all overlapping TAD boundaries”. Then, the regions outside of the boundaries were extracted using the “complementBed” function. The telomere/centromere regions were filtered using the “intersectBed -v” option. The resulting regions constituted the “all overlapping TAD boundaries”. Next, the TAD boundaries identified in MCF-10A and MCF-7 datasets were independently subtracted (by using the subtractBed function) from the “all overlapping TAD boundaries”. Within these two independently subtracted datasets, the TADs that have at least 90 % overlap ($-f$ 0.90 - r) were considered as “overlapping TADs”, TADs that were found only in MCF-7 were categorized as “MCF-7-specific TADs”, and the domains that were only found in MCF-10A subtracted datasets were categorized as “MCF-10A-specific TADs”.

Availability of supporting data

The raw and processed RNA-seq and Hi-C datasets have been submitted to NCBI Gene Expression Omnibus (GEO) under accession numbers [GEO:GSE71862 and GSE66733].

Additional files

Additional file 1: Supplementary Figure S1 to Figure S14. (PDF 23309 kb)

Additional file 2: A table listing the gene ontology terms of differentially expressed genes between MCF-10A and MCF-7 cells. (XLSX 8 kb)

Additional file 3: A table listing the gene ontology terms of the MCF-7 up-regulated genes that are on small chromosomes and are on compartment switch regions. (XLSX 5 kb)

Abbreviations

ALT: alternate lengthening of telomeres; Chr: chromosome; DMEM: Dulbecco's modified Eagle's medium; eQTL: expression quantitative trait locus; Hi-C: genome-wide chromosome conformation capture; ICE: iterative correction method; M-FISH: multiplex fluorescence in situ hybridization; SKY: spectral karyotyping; TAD: topologically associating domain.

Competing interests

The authors declare that they have no competing interests.

Authors' contributions

ARB, GSS, ANI, JLS, JBL, and AJvW conceived the project, ARB performed the Hi-C experiments, BL, RPM, and JD performed the initial Hi-C analysis, CET, DH, TLM, GB, and ARB generated the RNAseq data, CET and ARB analyzed the RNA-seq data, ARB performed the secondary Hi-C bioinformatic analyses with help from BL and RPM, all the authors discussed the results, ARB wrote the manuscript with input from all the authors. All authors read and approved the final manuscript.

Acknowledgments

We would like to thank Jeffrey A. Nickerson and Imbalzano and Stein lab members for critical discussion, Alper Kucukural for technical help with RNA-seq analysis, Seda Barutcu for critical reading of the manuscript and scientific input, Jonathan Gordon, Scott Tighe and Robert Devins for their help with deep sequencing. The next-generation sequencing was performed in the Advanced Genome Technologies Core Massively Parallel Sequencing Facility and was supported by the University of Vermont Cancer Center, Lake Champlain Cancer Research Organization, UVM College of Agriculture and Life Sciences, and the UVM College of Medicine. This work was supported by National Cancer Institute grant P01 CA082834 and Pfizer Investigator-Initiated Research Award - IIR Grant WS2049100.

Author details

¹Department of Cell and Developmental Biology, University of Massachusetts Medical School, 55 Lake Avenue North, Worcester, MA 01655, USA. ²Program in Systems Biology, University of Massachusetts Medical School, 55 Lake Avenue North, Worcester, MA 01655, USA. ³Department of Biochemistry and Molecular Pharmacology, University of Massachusetts Medical School, 55 Lake Avenue North, Worcester, MA 01655, USA. ⁴Department of Biochemistry & Molecular Biology, Mayo Clinic, 200 First Street SW, Rochester, MN 55905, USA. ⁵Department of Biochemistry and University of Vermont Cancer Center, University of Vermont College of Medicine, 89 Beaumont Avenue, Burlington, VT 05405, USA.

Received: 17 April 2015 Accepted: 3 September 2015

Published online: 28 September 2015

References

- Bickmore WA. The spatial organization of the human genome. *Annu Rev Genomics Hum Genet.* 2013;14:67–84.
- Bonora G, Plath K, Denholtz M. A mechanistic link between gene regulation and genome architecture in mammalian development. *Curr Opin Genet Dev.* 2014;27:92–101.
- de Laat W, Duboule D. Topology of mammalian developmental enhancers and their regulatory landscapes. *Nature.* 2013;502:499–506.
- Cancer Genome Atlas N. Comprehensive molecular portraits of human breast tumours. *Nature.* 2012;490:61–70.
- Stephens PJ, Tarpey PS, Davies H, Van Loo P, Greenman C, Wedge DC, et al. The landscape of cancer genes and mutational processes in breast cancer. *Nature.* 2012;486:400–4.
- Kandoth C, McLellan MD, Vandin F, Ye K, Niu B, Lu C, et al. Mutational landscape and significance across 12 major cancer types. *Nature.* 2013;502:333–9.
- Suvà ML, Riggi N, Bernstein BE. Epigenetic reprogramming in cancer. *Science.* 2013;339:1567–70.
- Zink D, Fischer AH, Nickerson JA. Nuclear structure in cancer cells. *Nat Rev Cancer.* 2004;4:677–87.
- Dey P. Cancer nucleus: morphology and beyond. *Diagn Cytopathol.* 2010;38:382–90.
- Gibcus JH, Dekker J. The hierarchy of the 3D genome. *Mol Cell.* 2013;49:773–82.
- Cremer T, Cremer M, Dietzel S, Müller S, Solovei I, Fakan S. Chromosome territories—a functional nuclear landscape. *Curr Opin Cell Biol.* 2006;18:307–16.
- Cremer M, von Hase J, Volm T, Brero A, Kreth G, Walter J, et al. Non-random radial higher-order chromatin arrangements in nuclei of diploid human cells. *Chromosome Res.* 2001;9:541–67.
- Bolzer A, Kreth G, Solovei I, Koehler D, Saracoglu K, Fauth C, et al. Three-dimensional maps of all chromosomes in human male fibroblast nuclei and prometaphase rosettes. *PLoS Biol.* 2005;3:e157.
- Cremer T, Cremer M. Chromosome territories. *Cold Spring Harb Perspect Biol.* 2010;2:a003889.
- Nye AC, Rajendran RR, Stenoien DL, Mancini MA, Katzenellenbogen BS, Belmont AS. Alteration of large-scale chromatin structure by estrogen receptor. *Mol Cell Biol.* 2002;22:3437–49.
- Meaburn KJ, Gudla PR, Khan S, Lockett SJ, Misteli T. Disease-specific gene repositioning in breast cancer. *J Cell Biol.* 2009;187:801–12.
- Meaburn KJ, Misteli T. Locus-specific and activity-independent gene repositioning during early tumorigenesis. *J Cell Biol.* 2008;180:39–50.
- Roix JJ, McQueen PG, Munson PJ, Parada LA, Misteli T. Spatial proximity of translocation-prone gene loci in human lymphomas. *Nat Genet.* 2003;34:287–91.
- Rocha PP, Micsinai M, Kim JR, Hewitt SL, Souza PP, Trimarchi T, et al. Close proximity to lgh is a contributing factor to AID-mediated translocations. *Mol Cell.* 2012;47:873–85.
- Zhang Y, McCord RP, Ho YJ, Lajoie BR, Hildebrand DG, Simon AC, et al. Spatial organization of the mouse genome and its role in recurrent chromosomal translocations. *Cell.* 2012;148:908–21.
- Lieberman-Aiden E, van Berkum NL, Williams L, Imakaev M, Ragoczy T, Telling A, et al. Comprehensive mapping of long-range interactions reveals folding principles of the human genome. *Science.* 2009;326:289–93.
- McCord RP, Nazario-Toole A, Zhang H, Chines PS, Zhan Y, Erdos MR, et al. Correlated alterations in genome organization, histone methylation, and DNA-lamin A/C interactions in Hutchinson-Gilford progeria syndrome. *Genome Res.* 2013;23:260–9.
- Seitan VC, Faure AJ, Zhan Y, McCord RP, Lajoie BR, Ing-Simmons E, et al. Cohesin-based chromatin interactions enable regulated gene expression within preexisting architectural compartments. *Genome Res.* 2013;23:2066–77.
- Dixon JR, Selvaraj S, Yue F, Kim A, Li Y, Shen Y, et al. Topological domains in mammalian genomes identified by analysis of chromatin interactions. *Nature.* 2012;485:376–80.
- Nora EP, Lajoie BR, Schulz EG, Giorgetti L, Okamoto I, Servant N, et al. Spatial partitioning of the regulatory landscape of the X-inactivation centre. *Nature.* 2012;485:381–5.
- Nora EP, Dekker J, Heard E. Segmental folding of chromosomes: a basis for structural and regulatory chromosomal neighborhoods? *Bioessays.* 2013;35:818–28.
- Giorgetti L, Galupa R, Nora EP, Piolot T, Lam F, Dekker J, et al. Predictive polymer modeling reveals coupled fluctuations in chromosome conformation and transcription. *Cell.* 2014;157:950–63.
- Le Dily F, Bau D, Pohl A, Vicent GP, Serra F, Soronellas D, et al. Distinct structural transitions of chromatin topological domains correlate with coordinated hormone-induced gene regulation. *Genes Dev.* 2014;28:2151–62.
- Fullwood MJ, Liu MH, Pan YF, Liu J, Xu H, Mohamed YB, et al. An oestrogen-receptor-alpha-bound human chromatin interactome. *Nature.* 2009;462:58–64.
- Li G, Ruan X, Auerbach RK, Sandhu KS, Zheng M, Wang P, et al. Extensive promoter-centered chromatin interactions provide a topological basis for transcription regulation. *Cell.* 2012;148:84–98.
- Hah N, Murakami S, Nagari A, Danko CG, Kraus WL. Enhancer transcripts mark active estrogen receptor binding sites. *Genome Res.* 2013;23:1210–23.
- Hsu PY, Hsu HK, Lan X, Juan L, Yan PS, Labanowska J, et al. Amplification of distant estrogen response elements deregulates target genes associated with tamoxifen resistance in breast cancer. *Cancer Cell.* 2013;24:197–212.
- Mourad R, Hsu PY, Juan L, Shen C, Koneru P, Lin H, et al. Estrogen induces global reorganization of chromatin structure in human breast cancer cells. *PLoS One.* 2014;9:e113354.
- Wang J, Lan X, Hsu PY, Hsu HK, Huang K, Parvin J, et al. Genome-wide analysis uncovers high frequency, strong differential chromosomal interactions and their associated epigenetic patterns in E2-mediated gene regulation. *BMC Genomics.* 2013;14:70.
- Osmanbeyoglu HU, Lu KN, Oesterreich S, Day RS, Benos PV, Coronello C, et al. Estrogen represses gene expression through reconfiguring chromatin structures. *Nucleic Acids Res.* 2013;41:8061–71.
- Barnett DH, Sheng S, Charn TH, Waheed A, Sly WS, Lin CY, et al. Estrogen receptor regulation of carbonic anhydrase XII through a distal enhancer in breast cancer. *Cancer Res.* 2008;68:3505–15.
- Bretschneider N, Kangaspekka S, Seifert M, Reid G, Gannon F, Denger S. E2-mediated cathepsin D (CTSD) activation involves looping of distal enhancer elements. *Mol Oncol.* 2008;2:182–90.
- Saramaki A, Diermeier S, Kellner R, Laitinen H, Vaisanen S, Carlberg C. Cyclical chromatin looping and transcription factor association on the regulatory regions of the p21 (CDKN1A) gene in response to 1alpha, 25-dihydroxyvitamin D3. *J Biol Chem.* 2009;284:8073–82.
- Matilainen JM, Malinen M, Turunen MM, Carlberg C, Vaisanen S. The number of vitamin D receptor binding sites defines the different vitamin D responsiveness of the CYP24 gene in malignant and normal mammary cells. *J Biol Chem.* 2010;285:24174–83.
- Wright JB, Brown SJ, Cole MD. Upregulation of c-MYC in cis through a large chromatin loop linked to a cancer risk-associated single-nucleotide polymorphism in colorectal cancer cells. *Mol Cell Biol.* 2010;30:1411–20.
- Zeitl MJ, Ay F, Heidmann JD, Lerner PL, Noble WS, Steelman BN, et al. Genomic interaction profiles in breast cancer reveal altered chromatin architecture. *PLoS One.* 2013;8:e73974.
- Dryden NH, Broome LR, Dudbridge F, Johnson N, Orr N, Schoenfelder S, et al. Unbiased analysis of potential targets of breast cancer susceptibility loci by Capture Hi-C. *Genome Res.* 2014;24:1854–68.
- Hughes JR, Roberts N, McGowan S, Hay D, Giannoulitou E, Lynch M, et al. Analysis of hundreds of cis-regulatory landscapes at high resolution in a single, high-throughput experiment. *Nat Genet.* 2014;46:205–12.
- Rousseau M, Ferraiuolo MA, Crutchley JL, Wang XQ, Miura H, Blanchette M, et al. Classifying leukemia types with chromatin conformation data. *Genome Biol.* 2014;15:R60.
- Misteli T. Higher-order genome organization in human disease. *Cold Spring Harb Perspect Biol.* 2010;2:a000794.
- Belton JM, McCord RP, Gibcus JH, Naumova N, Zhan Y, Dekker J. Hi-C: a comprehensive technique to capture the conformation of genomes. *Methods.* 2012;58:268–76.
- Lajoie BR, Dekker J, Kaplan N. The Hitchhiker's guide to Hi-C analysis: Practical guidelines. *Methods.* 2015;72:65–75.
- Imakaev M, Fudenberg G, McCord RP, Naumova N, Goloborodko A, Lajoie BR, et al. Iterative correction of Hi-C data reveals hallmarks of chromosome organization. *Nat Methods.* 2012;9:999–1003.
- Davidson JM, Goringe KL, Chin SF, Orsetti B, Besret C, Courtay-Cahen C, et al. Molecular cytogenetic analysis of breast cancer cell lines. *Br J Cancer.* 2000;83:1309–17.

50. Marella NV, Malyavantham KS, Wang J, Matsui S, Liang P, Berezney R. Cytogenetic and cDNA microarray expression analysis of MCF10 human breast cancer progression cell lines. *Cancer Res.* 2009;69:5946–53.
51. Kao J, Salari K, Bocanegra M, Choi YL, Girard L, Gandhi J, et al. Molecular profiling of breast cancer cell lines defines relevant tumor models and provides a resource for cancer gene discovery. *PLoS One.* 2009;4:e6146.
52. Dixon JR, Jung I, Selvaraj S, Shen Y, Antosiewicz-Bourget JE, Lee AY, et al. Chromatin architecture reorganization during stem cell differentiation. *Nature.* 2015;518:331–6.
53. Rao SS, Huntley MH, Durand NC, Stamenova EK, Bochkov ID, Robinson JT, et al. A 3D map of the human genome at kilobase resolution reveals principles of chromatin looping. *Cell.* 2014;159:1665–80.
54. Van Bortle K, Nichols MH, Li L, Ong CT, Takenaka N, Qin ZS, et al. Insulator function and topological domain border strength scale with architectural protein occupancy. *Genome Biol.* 2014;15:R82.
55. Pope BD, Ryba T, Dileep V, Yue F, Wu W, Denas O, et al. Topologically associating domains are stable units of replication-timing regulation. *Nature.* 2014;515:402–5.
56. Duggal G, Wang H, Kingsford C. Higher-order chromatin domains link eQTLs with the expression of far-away genes. *Nucleic Acids Res.* 2014;42:87–96.
57. Li Q, Seo JH, Stranger B, McKenna A, Pe'er I, Laframboise T, et al. Integrative eQTL-based analyses reveal the biology of breast cancer risk loci. *Cell.* 2013;152:633–41.
58. Barbieri M, Chotalia M, Fraser J, Lavitas LM, Dostie J, Pombo A, et al. A model of the large-scale organization of chromatin. *Biochem Soc Trans.* 2013;41:508–12.
59. Parada LA, McQueen PG, Munson PJ, Misteli T. Conservation of relative chromosome positioning in normal and cancer cells. *Curr Biol.* 2002;12:1692–7.
60. Chuang CH, Belmont AS. Moving chromatin within the interphase nucleus-controlled transitions? *Semin Cell Dev Biol.* 2007;18:698–706.
61. Therizols P, Illingworth RS, Courilleau C, Boyle S, Wood AJ, Bickmore WA. Chromatin decondensation is sufficient to alter nuclear organization in embryonic stem cells. *Science.* 2014;346:1238–42.
62. Draskovic I, Arnoult N, Steiner V, Bacchetti S, Lomonte P, Londono-Vallejo A. Probing PML body function in ALT cells reveals spatiotemporal requirements for telomere recombination. *Proc Natl Acad Sci U S A.* 2009;106:15726–31.
63. Heaphy CM, Subhawong AP, Hong SM, Goggins MG, Montgomery EA, Gabrielson E, et al. Prevalence of the alternative lengthening of telomeres telomere maintenance mechanism in human cancer subtypes. *Am J Pathol.* 2011;179:1608–15.
64. Debnath J, Muthuswamy SK, Brugge JS. Morphogenesis and oncogenesis of MCF-10A mammary epithelial acini grown in three-dimensional basement membrane cultures. *Methods.* 2003;30:256–68.
65. Song L, Florea L, Langmead B. Lighter: fast and memory-efficient sequencing error correction without counting. *Genome Biol.* 2014;15:509.
66. Li B, Dewey CN. RSEM: accurate transcript quantification from RNA-Seq data with or without a reference genome. *BMC Bioinformatics.* 2011;12:323.
67. Love MI, Huber W, Anders S. Moderated estimation of fold change and dispersion for RNA-seq data with DESeq2. *Genome Biol.* 2014;15:550.
68. Berriz GF, Beaver JE, Cenik C, Tasan M, Roth FP. Next generation software for functional trend analysis. *Bioinformatics.* 2009;25:3043-3044.
69. Shen L, Shao N, Liu X, Nestler E. ngs.plot: Quick mining and visualization of next-generation sequencing data by integrating genomic databases. *BMC Genomics.* 2014;15:284.
70. Sanyal A, Lajoie BR, Jain G, Dekker J. The long-range interaction landscape of gene promoters. *Nature.* 2012;489:109–13.
71. Quinlan AR. BEDTools: The Swiss-army tool for genome feature analysis. *Curr Protoc Bioinformatics.* 2014;47:11 12 11–34.

Submit your next manuscript to BioMed Central and take full advantage of:

- Convenient online submission
- Thorough peer review
- No space constraints or color figure charges
- Immediate publication on acceptance
- Inclusion in PubMed, CAS, Scopus and Google Scholar
- Research which is freely available for redistribution

Submit your manuscript at
www.biomedcentral.com/submit

